J Appl Electrochem (2009) 39:1975–1982
DOI 10.1007/s10800-009-9907-1

ORIGINAL PAPER

Electrochemical studies of Zn–Ni alloy coatings from acid chloride bath

S. Basavanna · Y. Arthoba Naik

Received: 14 February 2009 / Accepted: 14 April 2009 / Published online: 29 April 2009

Abstract The electrodeposition of Zn–Ni alloy from chloride bath was carried out in presence of condensation product (CP) formed between vanillin and hexamine. The investigation of electrodeposition and nucleation process was carried out on glassy carbon electrode using cyclic voltammetric and chronoamperometric techniques. During the anodic scan of cyclic voltammetry, three anodic peaks were observed corresponding to the dissolution of zinc and nickel from different phases of Zn–Ni alloy. The model of Scharifker and Hills was used to analyze the current transients and it revealed that Zn–Ni electrocrystallization process in the presence of CP, under the studied conditions, is governed by three-dimensional nucleation process controlled by diffusion. In presence of CP, the results indicated that nucleation process changes from progressive to instantaneous when the deposition potential becomes more negative. The phase structure and surface morphology of the deposits were characterized by means of X-ray diffraction analysis and Scanning electron microscopy, respectively.

Keywords Electrodeposition · Nucleation · Vanillin + hexamine · Zn–Ni alloy

1 Introduction

In recent years, great interest has been shown in the possibilities offered by the electrodeposition of alloys, mainly in the automotive industry [1–3]. Usually the mechanical and chemical properties of metals are improved by alloying. The electrodeposition of Zn–Ni alloys is interesting, because these alloys exhibit a significant higher corrosion resistance and better surface morphology than pure zinc [4–8]. The aeronautical industry has shown increasing interest in Zn–Ni alloy coating as a substitute for toxic and high-cost cadmium coatings [9]. The Zn–Ni alloys obtained by electrodeposition processes, with the amount of nickel varying between 8% and 14% by weight, give corrosion protection five to six times superior to that obtained with pure zinc deposits [10–12]. Although nickel is a more noble metal than zinc, the codeposition of Zn–Ni is anomalous [10, 13] and a higher percent of zinc is present in the final deposit. However, the crystallization nucleation and growth mechanism have not been studied in detail, especially in acid chloride Zn–Ni electroplating solutions.

Organic additives are often added into the plating bath of common metal (Zn, Ni, Co) to improve the properties of the final deposits and to make the surface more durable, uniform, and compact for better performances in terms of corrosion protection [14–16]. In the present study the condensation product of vanillin and hexamine has been selected as an organic additive for electrodeposition of Zn–Ni alloys from acid chloride bath.

2 Experimental

Zn–Ni deposits were obtained from a basic solution of 0.1 M $ZnCl_2$ + 0.05 M $NiCl_2.6H_2O$ in 2.5 M KCl + 0.32 M H_3BO_3 electrolyte, with a range of CP concentrations. The electrodeposition experiments were conducted at room temperature (298 K) in an unstirred solution. All the chemicals were of analytic grade and solutions were prepared using deionized water.

S. Basavanna · Y. Arthoba Naik (✉)
Department of Chemistry, School of Chemical Sciences, Kuvempu University, Shankaraghatta 577 451, India
e-mail: drarthoba@yahoo.co.in

Condensation product (CP) was synthesized from equimolar amounts of vanillin (1 mM) with chemical formula, $C_8H_8O_3$, and hexamine (1 mM) with chemical formula, $C_6H_{12}N_4$ (AR grade, s. d. fine chemicals), in ethanol medium (50 mL), under reflux condition for 3 h at 343 K [17]. The completion of the reaction was confirmed by thin layer chromatography (TLC).

The electrochemical measurements were performed with a commercial model EA-201 Electroanalyzer (ChemiLink system, Mumbai) with a three electrode system. A glassy carbon of geometrical area 0.05 cm^2, a platinum wire, and saturated calomel electrode were used as working, counter and reference electrodes respectively. Prior to each experiment, the working electrode was polished to a mirror finish with 0.05 μm alumina.

The composition and surface morphology of deposits were examined using an EDX analyzer integrated with scanning electron microscope (JEOL-JSM-6400). X-ray diffraction (XRD) study was used to determine the phases present in the alloy deposits. The X-ray diffractometer (PHILIPS-1710) with a CuKα radiation was employed to obtain XRD spectra using standard θ to 2θ geometry. The measurements were performed in the 2θ range of 30° to 80° with a tube voltage of 45 kV and current of 25 mA. JCPDS powder diffraction file cards were used for phase identification.

3 Results and discussions

3.1 Cyclic voltammetric (CV) studies

The electrochemical behavior of zinc and nickel was studied by using cyclic voltammetric technique. In these experiments, solutions containing 0.1 M $ZnCl_2$ and 0.05 M $NiCl_2 \cdot 6H_2O$ in 2.5 M KCl + 0.32 M H_3BO_3 with a range of CP concentrations were used.

The preliminary experiments showed that CP has no electrochemical activity under the experimental conditions used in this study. Figure 1 shows typical voltammograms obtained from alloy solutions with and without CP. The electrochemical behavior of Zn–Ni alloys was studied from a basic solution with a range of CP concentrations. The potential scan was started in the cathodic direction from the rest potential in the potential range from 0.2 to −1.75 V versus SCE.

During anodic scan two crossovers are observed between the current densities of the cathodic and anodic directions. The potential at which the more cathodic crossover occurs is known as the nucleation overpotential (E_η) [18]. The second cross over which occurs at −1.098 V versus SCE, is known as the crossover potential (E_{co}) [19]. The two crossovers are characteristic of process involving the nucleation [20].

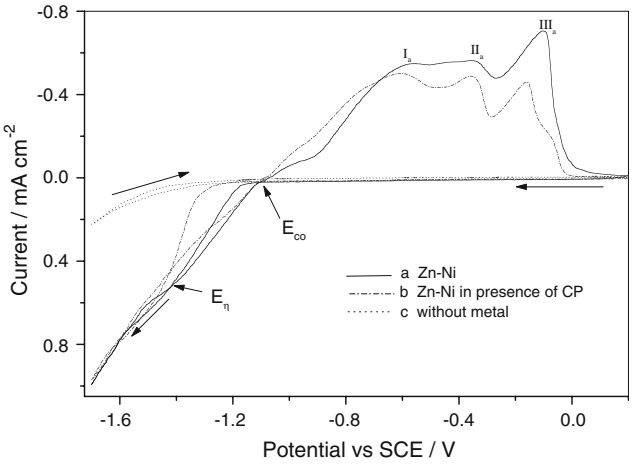

Fig. 1 Typical voltammograms obtained from 0.1 M $ZnCl_2$ + 0.05 M $NiCl_2 \cdot 6H_2O$ in 2.5 M KCl + 0.32 M H_3BO_3, pH 3.5, at different concentrations of CP: (*a*) 0.0 mM, (*b*) 0.2 mM, V = 30 mV s^{-1}. The supporting electrolyte 2.5 M KCl + 0.32 M H_3BO_3 + 0.2 mM CP is also shown

In the absence of CP, three oxidation peaks (I_a, II_a, and III_a) are observed in the potential range from –1.095 to 0.0 V versus SCE. The detection of multiple peaks during the electrochemical oxidation of alloys can be attributed to dissolution of the metals in the alloy via different intermediate phases [21]. The three anodic dissolution peaks for Zn–Ni alloy correspond to the dissolution of the constituents of two phases deposited, δ-phase (Ni_3Zn_{22}) and γ-phase (Ni_5Zn_{21}). The first (I_a) and second anodic peaks (II_a) correspond to the dissolution of zinc from δ- and γ-phases, respectively. The third peak (III_a) corresponds to the dissolution of Ni from their phases [22, 23]. Thus, the voltammetric response gives information regarding the characteristics of the components of the alloy and the structure of the deposited phases. The reduction potential shifts to more negative values in presence of CP in the basic solution. When the potential scan is reversed, three anodic peaks appear at the same range and the current densities of all the peaks decreases. These results indicated that the CP hinders the dissolution of Zn–Ni alloy and increases the corrosion resistance of the deposits.

3.2 Switching potentials (E_λ)

To identify the oxidation peaks, the voltammetry with switching potential technique was employed. The potential scan was started in the cathodic direction from the rest potential and was inverted at different potential values (switching potential, E_λ). E_λ values were chosen to be within the zone where the reduction processes are observed in the voltammograms. Figure 2 shows the voltammograms obtained from a solution without CP at different switching potentials (E_λ). When $E_{\lambda 4} = -1.6$ V versus

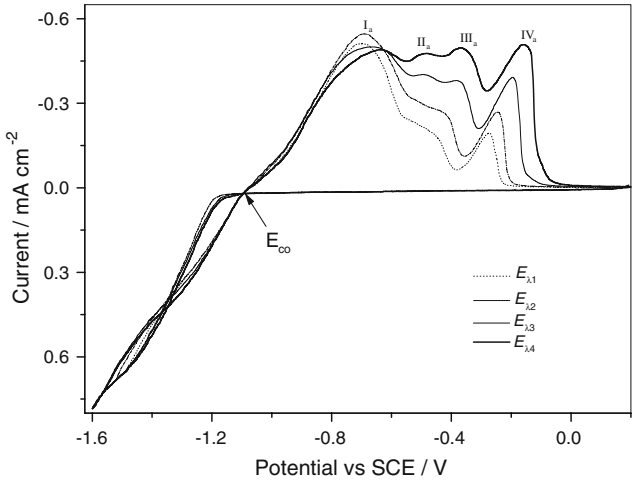

Fig. 2 Voltammograms obtained from 0.1 M $ZnCl_2$ + 0.05 M $NiCl_2 \cdot 6H_2O$ in 2.5 M KCl + 0.32 M H_3BO_3, pH 3.5, in the absence of CP at different values of E_λ: $E_{\lambda1} = -1.48$, $E_{\lambda2} = -1.52$, $E_{\lambda3} = -1.56$, $E_{\lambda4} = -1.60$ V versus SCE, V = 30 mV s^{-1}

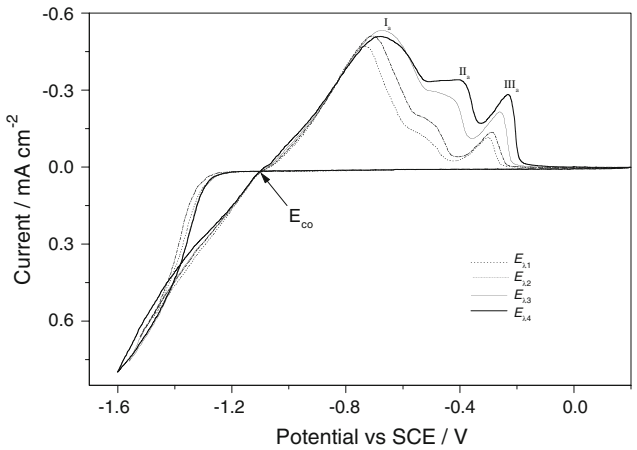

Fig. 3 Voltammograms obtained from 0.1 M $ZnCl_2$ + 0.05 M $NiCl_2 \cdot 6H_2O$ in 2.5 M KCl + 0.32 M H_3BO_3, pH 3.5, in the presence of CP at different values of E_λ: $E_{\lambda1} = -1.48$, $E_{\lambda2} = -1.52$, $E_{\lambda3} = -1.56$, $E_{\lambda4} = -1.60$ V versus SCE, V = 30 mV s^{-1}

SCE, four anodic peaks (I_a, II_a, III_a, and IV_a) are observed, corresponding to the oxidation of Zn–Ni alloy. The first dissolution of anodic peak at −0.686 V, attributed to the dissolution of zinc from pure Zn phase. The second dissolution peak at −0.498 V and third peak at −0.367 V, correspond to the dissolution of zinc from δ- and γ-phases, respectively which was verified by XRD. Fourth peak at −0.16 V corresponds to the dissolution of nickel from two phases of Zn–Ni alloy. At $E_{\lambda2} = -1.52$ and $E_{\lambda1} = -1.48$ V versus SCE, three anodic peaks are observed due to the absence of δ-phase. When $E_\lambda > -1.48$ V versus SCE, zinc metal is preferentially deposited with respect to nickel, as would be expected for a process involving anomalous co-deposition of Zn–Ni alloy [24–26].

A similar study was carried out on solutions containing CP of concentration 0.2 mM. The results obtained at different values of E_λ in the range of −1.56 to −1.48 V versus SCE are shown in Fig. 3. When $E_{\lambda4} = -1.6$ V versus SCE, only three oxidation peaks are observed. An important feature of results presented above is that the oxidation of zinc from δ-phase is not observed. These studies show that at higher potentials ($E_\lambda > -1.48$ V vs SCE), zinc metal is preferentially deposited with respect to nickel. The Fig. 3 shows that, E_{co} is independent of E_λ. The mean value of E_{co} was −1.098 versus SCE/V, which is close to the conditional potential of the $ZnCl_4^{2-}/Zn(0)$ system $\left(E^1_{ZnCl_4^{2-}/Zn(0)} = -1.094\,\text{vs. SCE/V}\right)$. These results indicate that the reduction processes involve the soluble species $ZnCl_4^{2-}$, and from this, it can be concluded that CP does not form complexes with Zn^{2+} in agreement with previously obtained results [27]. The CP adsorbs on the cathode surface affect the activation energy and rate of charge transfer in the electrochemical reaction, and may also influence the mechanism of electrocrystallization.

3.3 Transient analysis

The chronoamperometric studies were used to identify the Zn–Ni nucleation mechanism at different potentials. This

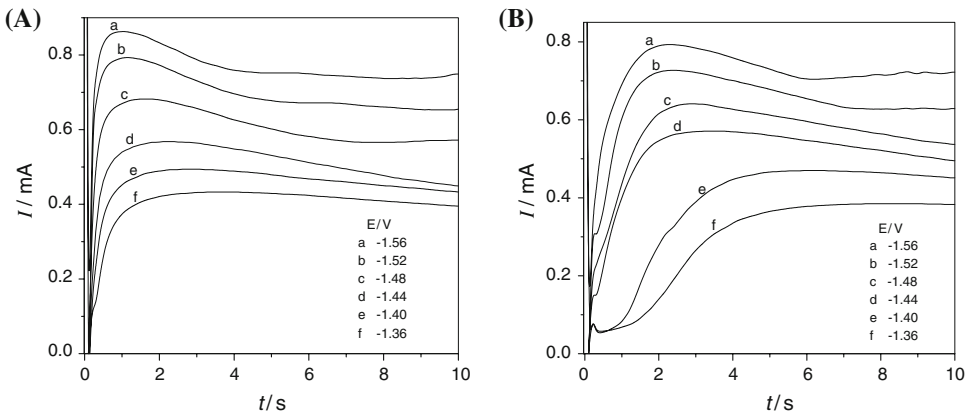

Fig. 4 Current transients for Zn–Ni deposition from 0.1 M $ZnCl_2$ + 0.05 M $NiCl_2 \cdot 6H_2O$ in 2.5 M KCl + 0.32 M H_3BO_3, pH 3.5, **a** in the absence and **b** in the presence of 0.2 mM CP

potentiostatic technique has proved to be a powerful tool for elucidating the mechanisms by which new phases form (electrocrystallization) [28]. Figures 4 a and b show the potentiostatic current versus time (I–t) transients recorded during the reduction of Zn–Ni alloy in the potential range between −1.36 and −1.56 V versus SCE, in absence and presence of CP. The behavior of these transients is typical of a nucleation process with three-dimensional growth of a nuclei limited by the diffusion of the electroactive species. The transients can be divided into three regions: In the first region, which corresponds to short times ($t < 0.5$ s), the decrease in the cathodic current density is related to the charging of the double layer. The second region corresponds to the increase in cathodic current density up to a maximum, which is typical of crystal nucleation and growth processes. The third region corresponds to the decline in the current density which is typical of a diffusion-controlled process.

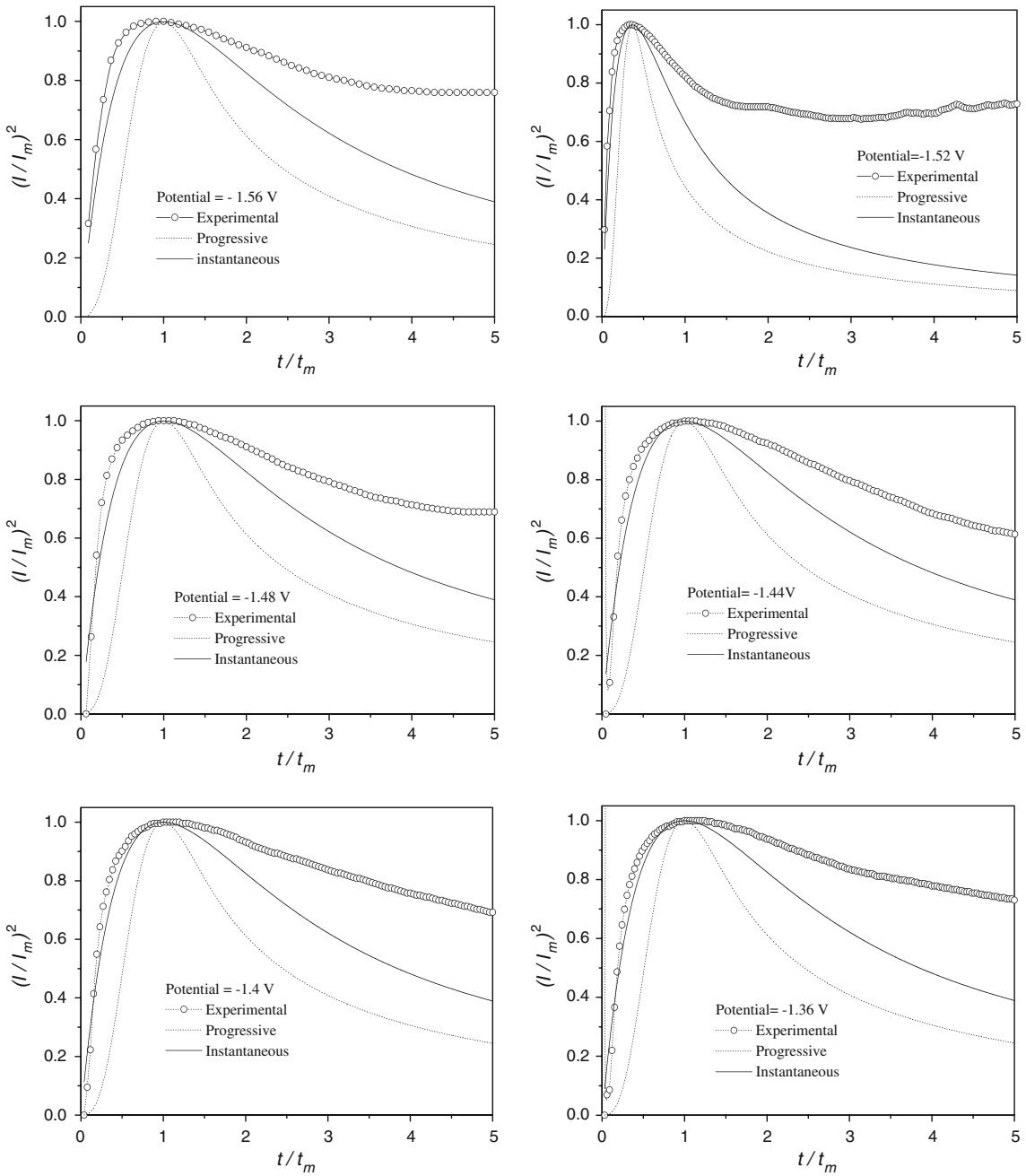

Fig. 5 Non-dimensional j/j_{max} versus t/t_{max} plot for electrodeposition of Zn–Ni alloy coating in absence of CP

Comparing Figs. 4a and b, for the same final potential, I_{max} is lower and t_{max} larger, in the presence of CP. This fact seems to indicate that the CP hinders the nucleation process.

These transients were normalized to $(I/I_{max})^2$ versus t/t_{max} and then compared to the well known theoretical $(I/I_{max})^2$ versus t/t_{max} curves derived for instantaneous and progressive three-dimensional (3D) nucleation/growth models [29], whose equations are given for instantaneous nucleation:

$$\left(\frac{I}{I_{\max}}\right)^2 = \frac{1.9542}{t/t_{\max}}\left\{1-\exp\left[-1.2564\left(\frac{t}{t_{\max}}\right)\right]\right\}^2 \quad (1)$$

and for progressive nucleation

$$\left(\frac{I}{I_{\max}}\right)^2 = \frac{1.2254}{t/t_{\max}}\left\{1-\exp\left[-2.3367\left(\frac{t}{t_{\max}}\right)^2\right]\right\}^2 \quad (2)$$

Non dimensional plots obtained with the experimental and theoretical data for Zn–Ni alloy deposition in the

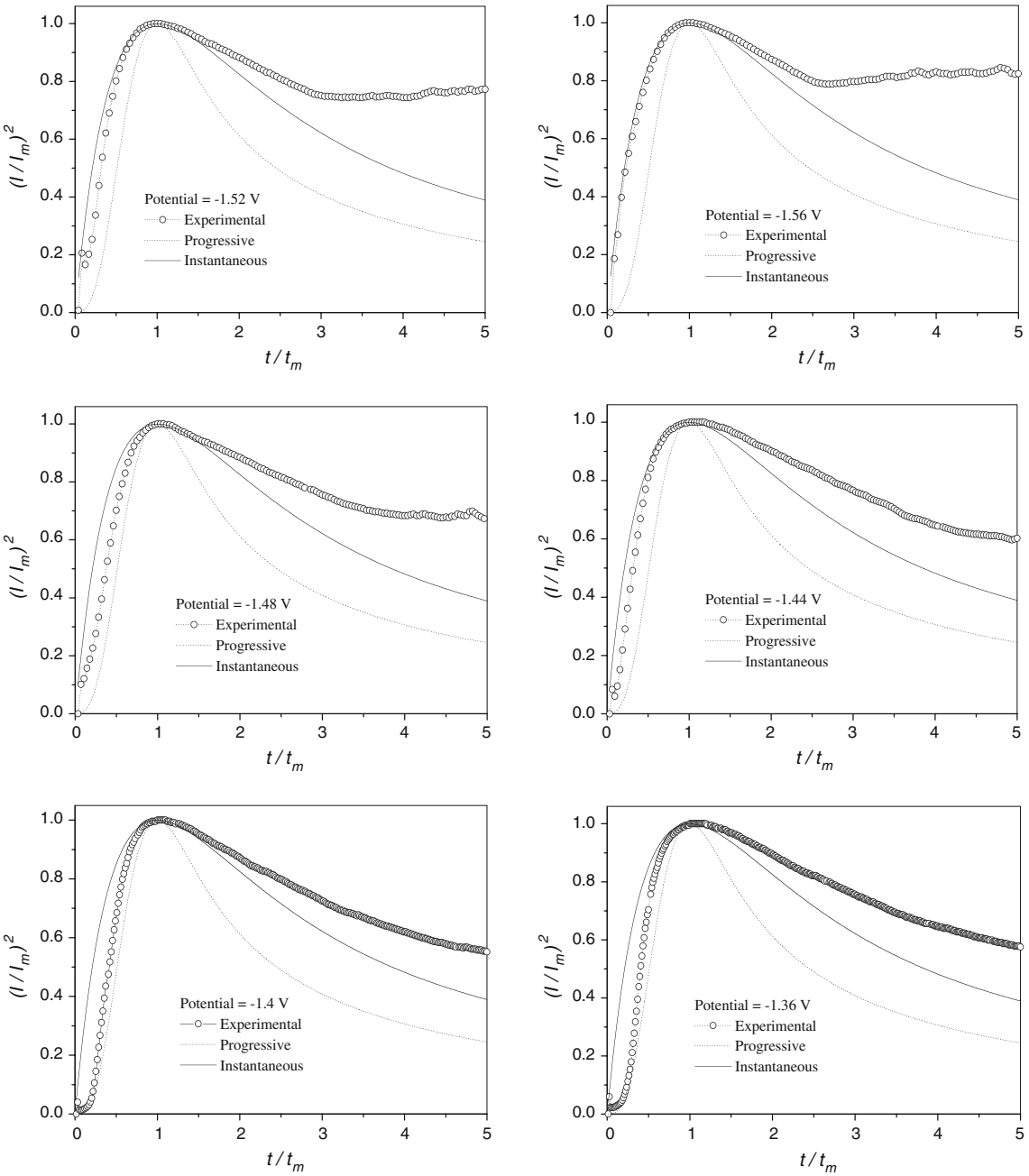

Fig. 6 Non-dimensional j/j_{max} versus t/t_{max} plot for electrodeposition of Zn–Ni alloy coating in presence of 0.2 mM CP

absence and in the presence of CP are shown in Figs. 5 and 6, at different potentials, respectively.

From Figs. 5 and 6, it can be seen that, after the current maximum, the experimental $(I/I_m)^2$ is much larger than that calculated from the theoretical model. According to the well accepted theorem that the electrochemical reduction of iron-group metal ions on the cathode surface keeps to the following mechanism [30].

$$2H_2O + 2e^- \rightarrow H_2 + 2OH^- \quad (3)$$

$$M^{2+} + OH^- \rightarrow M(OH)^+ \quad (4)$$

$$M(OH)^+ \rightarrow M(OH)^+_{ads} \quad (5)$$

$$M(OH)^+_{ads} + 2e^- \rightarrow M + OH^- \quad (6)$$

where M designates iron, cobalt, and nickel atoms. The reduction rate of M mainly depends on the stability of $M(OH)^+_{ads}$ or $M(OH)^+$. The stability of the zinc and nickel metal monohydroxide ions or metal hydroxides can be sorted in the following order: $Ni(OH)^+ > Zn(OH)^+$ as elucidated above, the content of nickel in the electrodeposited coating is much lower than that in the electroplating solution and the concentration of Ni^{2+} in the vicinity of the cathode should maintain a relatively steady value during the whole electroplating process. Meanwhile the nucleation/growth process of Zn–Ni deposit was always coupled with the evolution of hydrogen, which can be seen from the Eqs. (3) and (6). Consequently, the experimental $(I/I_m)^2$ should be much larger than that calculated from the theoretical model.

In the Fig. 5 the rising part of the transients located nearer to the instantaneous nucleation at lower potentials. As soon as the potential turns to more negative values, the curves does not confirm to either of the models of diffusion-controlled 3D nucleation in absence of CP.

Figure 6 shows the nucleation mechanism of Zn–Ni alloy deposition in presence of CP. At lower potentials the normalized curves located between theoretical progressive and instantaneous nucleation. As soon as final potential changes to more negative values, the nucleation process confirms the instantaneous nucleation process. These results confirm that as soon as zinc being incorporated to the deposits the nucleation process is modified. The nucleation process may occur by instantaneous or progressive nucleation in presence of CP, depending on the final potential.

3.4 SEM analysis

The nature of crystal growth in presence and absence of addition agents is explained with the help of SEM photomicrographs and shown in Fig. 7. Figure 7a is the SEM photomicrograph of the deposit obtained from the Zn–Ni basic solution showing coarse–grained deposit having non-uniform crystal size. Increase in additive concentration, increases the refinement of crystal size, regulates the uniform arrangement of crystals and hence results in the fine-grained deposits (Fig. 7d). The SEM cross sectional image (Fig. 8) of Zn–Ni coating obtained in presence of CP shows that the thickness of the coating is 6 μm. EDX analysis performed on the deposit obtained in presence of CP revealed that the deposit contains 4% nickel and remaining zinc.

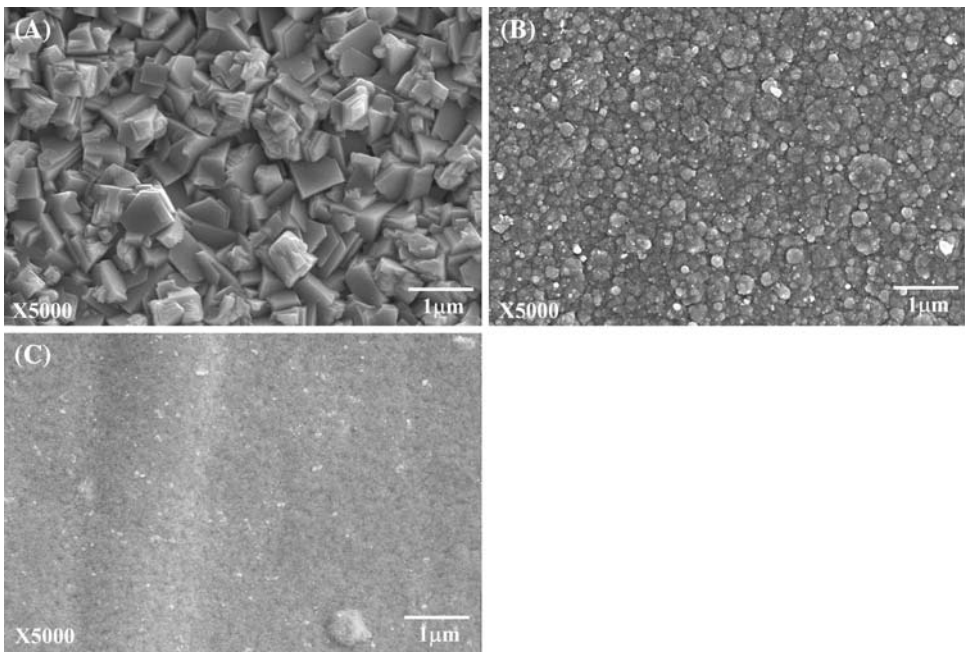

Fig. 7 SEM images of coatings obtained from base solutions with different CP concentrations: (**a**) 0.0, (**b**) 0.1 and (**c**) 0.2 mM

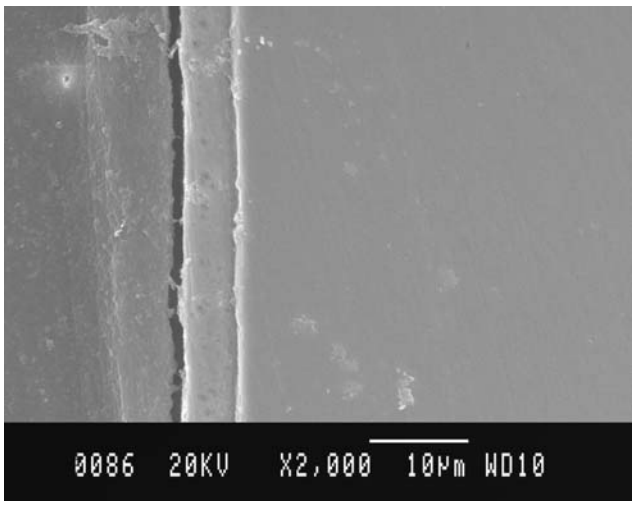

Fig. 8 SEM cross-section image of Zn–Ni coating obtained in presence of CP

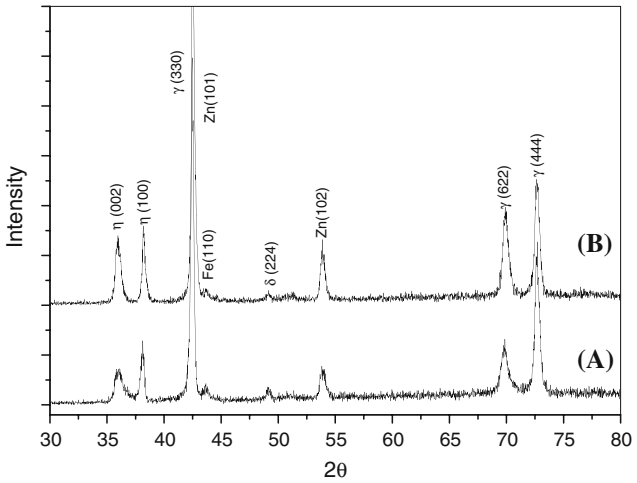

Fig. 9 X-ray diffraction patterns of electrodeposits of Zn–Ni from solutions (*a*) in absence and (*b*) in presence of 0.2 mM CP

3.5 X-ray diffraction (XRD) analysis

The XRD pattern shows (Fig. 9) the formation of lines corresponding to η-phase Zn(101) and additional lines that can be indexed considering a γ-Ni_5Zn_{21} and δ-Ni_3Zn_{22}. In addition, an increase is observed in the intensity of γ-Ni_5Zn_{21} phase lines as the concentration of CP increases from 0.0 to 0.2 mM. The increase of γ-Ni_5Zn_{21} phase content in the deposit increases the corrosion resistance of the alloy [22]. Therefore these results revealed that the Zn–Ni deposits obtained in presence of CP, exhibited higher corrosion resistance.

4 Conclusions

The protective Zn–Ni coating was obtained from the acid chloride bath, and corresponding electroplating behavior was investigated using cyclic voltammetry and chronoamperometric methods in conjunction with SEM and XRD techniques. Voltammetric studies show that at higher switching potential, three anodic peaks were observed corresponding to the dissolution of zinc from two phases (δ- and γ-phase) and dissolution of nickel from their phases. In the high deposition overpotential, the electrodeposition of Zn–Ni coating in presence of CP followed 3D nucleating and subsequent instantaneous grain growth mechanism, while in the case of low deposition overpotential; it followed 3D nucleating and subsequent progressive grain growth mechanism. XRD studies showed that the deposit containing mainly γ- and η-phases of Zn–Ni alloy. SEM analysis of the coating morphologies showed that fine-grained deposits form in the presence of CP, promoting the formation of smooth and shiny coatings.

Acknowledgment The authors are grateful to the Kuvempu University and University Grants Commission, New Delhi, for providing the facilities and financial support to carryout this work.

References

1. Ramanauskas R (1999) Appl Surf Sci 153:53
2. Winand R (1991) J Appl Electrochem 21:377
3. Wilcox GD, Gabe DR (1993) Corros Sci 35:1251
4. Pushpavanam M, Natarajan SR, Balakrishnan K, Sharma LR (1991) J Appl Electrochem 21:642
5. Kautek W, Sahre M, Paatsch W (1994) Electrochim Acta 39:1151
6. Muller C, Sarret M, Benballa M (2002) J Electroanal Chem 519:85
7. Beltowska-Lehman E, Ozga P, Swiatek Z, Lupi C (2002) Surf Coat Technol 151:444
8. Shivakumara S, Manohar U, Arthoba Naik Y, Venkatesha TV (2007) Bull Mater Sci 30(5):455
9. Alfantazi AM, Page J, Urb U (1996) J Appl Electrochem 26:1225
10. Hall DE (1983) Plating Surf Finish 70:59
11. Gavrila M, Millet JP, Mazille H, Marchandise D, Cuntz JM (2000) Surf Coat Technol 123:164
12. Garcia J, Barcelo G, Sarret M, Muller C, Pregonas J (1994) J Appl Electrochem 24:1249
13. Brenner A (1963) Electrodeposition of alloys, vol 1. Academic Press, New York
14. Muralidhara HB, Arthoba Naik Y, Sachin HP, Venkatesha TV (2008) Indian J Chem Technol 15:155
15. Arthoba Naik Y, Venkatesha TV (2005) Bull Mater Sci 28(5):495
16. Muralidhara HB, Arthoba Naik Y (2008) Surf Coat Technol 202:3403
17. Chen D, Martell AE (1987) Inorg Chem 26:1026
18. Fletcher S (1983) Electrochim Acta 28:917
19. Fletcher S, Halliday CS, Gates D, Westcott M, Lwin T, Nelson G (1983) J Electroanal Chem 159:267
20. Gunawardena G, Hills G, Montenegro I (1982) J Electroanal Chem 138:241

21. Jovic VD, Zejnilovic RM, Despic AR, Stevanoic JS (1998) J Appl Electrochem 18:511
22. Abou-Krisha MM (2005) Appl Surf Sci 252:1035
23. Abou-Krisha MM, Rageh HM, Matter EA (2008) Surf Coat Technol 202:3739
24. Ashassi-Sorkhabi H, Hagrah A, Parvini-Ahmadi N, Manzoori J (2001) Surf Coat Technol 140:278
25. Petrauskas A, Grinceviciene L, Cesuniene A, Juskenas R (2006) Electrochim Acta 51:4204
26. Soares ME, Souza CAC, Kuri SE (2006) Surf Coat Technol 201:2953
27. Diaz-arista P, Meas Y, Ortega R, Trejo G (2005) J Appl Electrochem 35:217
28. Trejo G, Ortega R, Meas Y, Chainet E, Ozil P (2003) J Appl Electrochem 33:373
29. Scharifker BR, Hills G (1983) Electrochim Acta 28:879
30. Tsay P, Hu CC (2002) J Electrochem Soc 149:C492